Article

Identification of ACE2 as the Entry Receptor for Two Novel European Bat Merbecoviruses

Chengbao Ma[1,#], Chen Liu[1,#], Qing Xiong[1], Xiao Yu[1], Yuanmei Chen[1], Junyu Si[1], Peng Liu[1], Fei Tong[1], Meiling Huang[1], Huan Yan[1,*]

[1] State Key Laboratory of Virology, Institute for Vaccine Research and Modern Virology Research Center, College of Life Sciences, TaiKang Center for Life and Medical Sciences, Wuhan University, Wuhan, Hubei, 430072, China.

[#] These authors contributed equally to this work.

[*] Correspondence: huanyan@whu.edu.cn

Address: Luojia Mountain, Wuchang District, Wuhan 430072, China

Abstract

The unknown identity of the entry receptors utilized by many coronaviruses has significantly impeded our comprehensive understanding of these important pathogens. We recently reported an unexpected usage of angiotensin-converting enzyme 2 (ACE2), instead of Dipeptidyl peptidase-4 (DPP4), for cellular entry by NeoCoV and PDF-2180, close relatives of MERS-CoV that infect African bats. However, the presence and distribution of other ACE2-using merbecoviruses remain enigmatic. In this study, through sequence and structural analyses, we predicted that two newly discovered merbecoviruses infecting European Pipistrellus bats (*Pipistrellus nathusii*), namely MOW-15-22 and PnNL2018B, may also utilize ACE2 as their receptors. Functional profiling of 103 ACE2 orthologues from a variety of mammals confirmed that several ACE2 from bats efficiently facilitate the entry of MOW-15-22 and PnNL2018B. Conversely, no binding or entry signals for both viruses were detected when assessing seven DPP4 orthologues from humans, hedgehogs, and bats. Characterization of Pteronotus davyi (P.dav) ACE2 mediated entry of MOW-15-22 reveals a significant exogenous protease dependence, which can be dose-dependently neutralized by soluble P.dav ACE2 recombinant protein and a broadly neutralizing S2-targeting antibody. Verification of the previously reported critical ACE2 determinants for NeoCoV recognition reveals that MOW-15-22 and PnNL2018B displayed a glycan-independent binding mode with significantly altered interaction details. This study sheds light on two additional ACE2-using merbecoviruses circulating among European bats and underscores the potential zoonotic risk associated with these viruses.

Keywords: Bats, Receptor, MOW-15-22, PnNL2018B, ACE2, Merbecoviruses, Host tropism

Introduction

The COVID-19 pandemic has underscored the critical need for close monitoring the zoonotic spillover of animal coronaviruses, particularly those originating from bat species (Chiroptera), known as the primary natural reservoirs for at least hundreds of α and β-coronaviruses[1-8]. Notably, the three high pathogenic human coronaviruses, SARS-CoV, SARS-CoV-2, and MERS-CoV, all belong to the β-coronaviruses genus[5,9,10]. MERS-CoV, classified under the merbecoviruses subgenus, is the causative agent for the Middle East respiratory syndrome with a case-fatality rate of 36%, which caused sporadic transmission since its outbreak in 2012 [11]. Although dromedary camels have been well documented as intermediate host of MERS-CoV, the evolutionary origin of this virus remains unclear and has been linked to potential recombinations in bat merbecoviruses [12-17].

The viral receptor is a key host factor for viral entry, determining tissue tropism, host range, and transmission efficiency of viruses[18-21]. Thus far, ACE2 and DPP4 have been widely acknowledged protein receptors for β-coronaviruses. both are engaged by the C-terminal domain (or domain B) of subunit 1 (S1-CTD) of viral spike proteins[22,23]. Typically, ACE2 is considered the primary entry receptor for sarbecoviruses, whereas DPP4 is thought to mediate entry for many merbecoviruses, although uncharacterized receptor usage has been found in viruses from both subgenus[5,24-31]. However, recent discoveries have challenged these notions. NeoCoV and PDF-2180, two close relatives of MERS-CoV found in African bats, employ a novel interaction mode to recognize ACE2 as their functional receptors, revealing a receptor usage promiscuity among merbecoviruses[32]. While these two viruses exhibit limited efficiency in using human ACE2 (hACE2), a single mutation (e.g., T510F) in the receptor binding motif (RBM) enhances their ability to enter human cells. Moreover, NeoCoV and PDF-2180 display a broad ACE2 recognition spectrum across various mammals, underscoring a relatively high zoonotic risk[32,33].

Nonetheless, the receptors for many merbecoviruses, including hedgehog coronaviruses (EriCoVs) such as HKU31, as well as several other bat coronaviruses like HKU5, MOW-15-22, and PN-βCoV remain elusive[29,34-36]. Previous studies have suggested that HKU5 and HKU31 may not use DPP4 or ACE2 as their receptors, leaving their entry receptor identities to be determined.

MOW-15-22 and PN-βCoV are two bat merbecoviruses recently identified in *P. nathusii* bats, a bat species commonly found in Europe[35,36]. To avoid confusion, we designated a specific virus of PN-βCoV (Betacoronavirus sp. isolate BtCoV/P.nathusii/NL/2018-403.3) as PnNL2018B in this study since both viruses are β-CoVs infecting the same host. MOW-15-22 was discovered in the Mosco region, while the PnNL2018B was identified in bats residing in the Netherlands with complete genome sequenced, although its relative VM314 (defined based on a sequence fragment in its RNA-dependent RNA polymerase) has been reported as early as in 2010[37]. Notably, some studies have proposed that DPP4 may serve as the entry receptor for MOW-15-22 and PnNL2018B based on molecular docking analyses.

In this study, we demonstrated that two recently reported European merbecoviruses, MOW-15-22 and PnNL2018B, with considerable genetic differences with the previously identified ACE2-using merbecoviruses, also utilize bat ACE2 rather than DPP4 as their functional receptors through a series of cellular and biochemical experiments. Our findings suggest that the diversity of ACE2-using merbecoviruses may be broader than previously recognized, raising concerns about the potential human emergence of these viruses.

Results

Phylogenetic and structural analyses suggest ACE2 usage by MOW-15-22 and PnNL2018B

Recently, two novel bat merbecoviruses with complete genome sequenced, MOW-15-22 and PN-βCoV (designated PnNL2018B in this study), were independently reported by research teams in Russia and Netherlands[35,36] (**Fig. 1a**). Both viruses were discovered in *P. nathusii*, a bat species inhabiting a wide range of Europe and undertakes a seasonal long-distance migration, usually from northeast to southwest Europe (**Fig. 1b**)[38,39]. In our quest to identify receptors for representative merbecoviruses, we noticed these two viruses form a distinct clade and exhibited an unknown receptor usage. At the complete-genome level, MOW-15-22 and PnNL2018B share less genetic similarity with the African bat coronaviruses NeoCoV and PDF-2180 but show greater genetic homology with a Italian bat merbecovirus (Hsavll/Italy/206645-40/2011) and a DPP4-using virus HKU25[35,40](**Fig. 1c**). However, their RBD sequences from these viruses cluster with the ACE2-using NeoCoV/PDF-2180 and an Asian hedgehog virus HKU31 (**Fig. 1d**). Aligning of equivalent sequences based on the NeoCoV receptor binding motif (RBM) reveals a relatively variable region

with low conservation, signifying uncertainty regarding receptor usage **(Fig. 1e)**. Importantly, the MOW-15-22 and PnNL2018B possess two insertions at the putative RBM compared to other merbecoviruses, potentially significantly influencing receptor interactions. Notably, the AlphaFold-predicted RBD structures of MOW-15-22 and PnNL2018B more closely resemble the ACE2-utilizing merbecoviruses NeoCoV and PDF-2180 in view of the presence of an helix region within the RBM, albeit with elongated putative receptor binding loops (**Fig. 1f**). Simplot analysis queried by MERS-CoV genome sequences demonstrates that the RBD regions of MOW-15-22 and PnNL2018B display lower similarity to MERS-CoV compared to the DPP4-using HKU4 (**Fig. 1g**). Collectively, these data suggest potential ACE2 usage by MOW-15-22 and PnNL2018B, eventhough they are phylogenetic distant from NeoCoV and PDF-2180 at the whole-genome level.

Multi-species ACE2 usage spectrum of MOW-15-22 and PnNL2018B

To determine whether MOW-15-22 and PnNL2018B utilize ACE2 as their receptors, we conducted a series of cell-based experiments to evaluate the functionality of various ACE2 orthologue in facilitating viral RBD binding and pseudovirus entry. As the complete genome sequences or coding sequences of ACE2 and DPP4 orthologues from *P. nathusii* are currently unavailable, we utilized a well-characterized receptor library consisting of 103 ACE2 and 7 DPP4 orthologues from 52 bats and 53 non-bat mammals to comprehensively assess RBD binding and pseudovirus entry efficiency[33]. These assays were carried out in 293T cells transiently transfected with plasmids expressing the receptors, all of which were previously confirmed to be properly expressed.. Our findings indicate that MOW-15-22 pseudovirus entry occurred in cells expressing bat ACE2 from P. par, P. dav, L. bor, and several other bat species, while the the PnNL2018B pseudovirus entry was supported by bat ACE2 from L. bor, N. hum, P. pip, and several other bat species (**Fig. 2a)**. Notably, in contrast to NeoCoV and PDF-2180, which exhibit a broad potential host tropism, both MOW-15-22 and PnNL2018B were incapable of efficiently utilizing ACE2 from non-bat mammals **(Fig. 2b).** Although we lack ACE2 binding data from the host species P. nat, we observe efficient RBD binding of MOW-15-22 in cells expressing two ACE2 orthologues from the *Pteronotus* genus (P. dav and P. par) (**Fig. 2a**). Furthermore, no binding or entry signal was detected in cells expressing human ACE2 and several DPP4 orthologues from the indicated species (**Fig. 2c-g**). It's important to note that the observed inconsistency between RBD binding and viral entry is a phenomenon commonly observed

in other coronaviruses, including NeoCoV/PDF-2180 and SARS-CoV/SARS-CoV-2[32,41]. One possible explanation for this phenomenon is that RBD binding is dynamic, whereas pseudotype entry is a cumulative event. Consequently, some receptors with kinetic features of fast association and fast dissociation can mediate efficient entry but may not exhibit strong binding in end-point binding assays. Indeed, the relative entry efficiency is also greatly influenced by the presence of exogenous trypsin (**Fig. 2h-j**), which is believed to lower the energy barrier and facilitate viral entry[42]. Therefore, ACE2 orthologues that are less efficient in supporting viral binding, such as L. bor ACE2, exhibited significantly higher dependence on the presence of TPCK-treated trypsin (**Fig. 2j**).

Characterization of bat ACE2-mediated entry of novel ACE2-using merbecoviruses

We proceeded to characterize the functionality of representative bat ACE2 in mediating the infection of these European merbecoviruses. A live-cell immunofluorescence-based RBD-hFc binding assay demonstrated that P.dav and P.par ACE2 efficiently facilitated the RBD binding of MOW-15-22 (**Fig. 2a**). Flow cytometry was subsequently conducted to confirm specific RBD binding supported by the ACE2 orthologues from P.dav and P.par, with human ACE2 (hACE2) as a negative control **(Fig. 3a).** Binding kinetics between MOW-15-22 RBD and P.dav or human ACE2 were analyzed using the Biolayer Interferometry (BLI). In general, P.dav ACE2 exhibited rapid association with MOW-15-22 RBD. However, the dissociation of P.dav ACE2 from MOW-15-22 RBD was also fast compared to the P.pip ACE2-NeoCoV RBD complex, resulting in a KD of approximately 10 nM (**Fig. 3b**). By contrast, no binding signal was detected between human ACE2 and MOW-15-22 RBD (**Fig. 3c**).

We further investigated the viral spike-mediated cell-cell membrane fusion assisted by different ACE2 orthologues. The two novel ACE2-using viruses lack furin cleavage sites at the S1/S2 junction (**Fig. S1**). Consequently, MOW-15-22 exhibited a prominent trypsin-dependent membrane fusion phenotype in bat ACE2-expressing cells, as was similarly observed in NeoCoV and PDF-2180[32] (**Fig. 3d-e**). Notably, although L.bor ACE2 failed to support detectable MOW-15-22 RBD binding, its expression and interaction with MOW-15-22 spike proteins induced a considerable amount of membrane fusion in the presence of exogenous trypsin (**Fig. 3d-e**). We also investigated whether the entry of ACE2-using viruses could be neutralized by interfering with the viral-receptor interaction. We demonstrated that viral entry could be efficiently inhibited by recombinant soluble ACE2 or

MOW-15-22 RBD-hFc fusion proteins (**Fig. 3f, and S2)**. Additionally, we evaluated the potency of MERS-CoV RBD-specific nanobodies and pan-β-CoV broadly neutralizing S2 antibodies targeting the stem helix (S2P6) or the S2' cleavage site/fusion peptide (76E1) (**Fig. 3g-i**)[43,44]. However, neither the MERS-CoV RBD-specific nanobodies nor S2P6 cross-reacted with MOW-15-22 or PnNL2018B to show inhibitory activity. This might be attributed to the discrepancy of equivalent sequences from these viruses in the S2P6 epitope compared with that of SARS-CoV-2 (**Fig. 3j**). Nevertheless,, 76E1 maintained its potency to neutralize the entry of these viruses due to the conservation of the critical residues in this epitope across these merbecoviruses (**Fig. 3k**).

Glycan-independent ACE2 recognition by MOW-15-22

Previous investigations into the interaction between P.pip ACE2 and NeoCoV/PDF-2180 revealed a unique glycan-dependent ACE2 binding mode[32]. Four molecular determinants, designated A to D, located in the binding interface in ACE2 were demonstrated crucial for species-specific ACE2 recognition. Among them, determinants A and C carry glycosylation sites, while determinants B and D are characterized by critical residues capable of forming salt bridges in P.pip ACE2 (**Fig. 4a**). Probably due to the RBM sequence variation, molecular docking did not provide a convincing interaction model for MOW-15-22 and P.dav ACE2 complex **(Fig. S3)**. Nevertheless, sequence analysis of P.dav and P.par ACE2 indicated that P.dav ACE2 shares similar residues with NeoCoV within these determinants, while P.par contains unfavorable residues in determinants B and C for NeoCoV interaction. Therefore, several P.dav and P.par ACE2 mutants carrying theoretically unfavorable residues, as indicated in previous studies based on NeoCoV, were generated to test the involvement of these determinants in MOW-15-22 receptor recognition **(Fig. 4b)**. Immunofluorescence and immunoblotting assays indicated that these mutants were expressed at similar levels **(Fig. 4c,e)**. As expected, introducing unfavorable residues within these determinants impaired NeoCoV RBD binding and pseudovirus entry. However, all these mutants maintained their receptor functionality for MOW-15-22, including P.par-T56I ACE2, which lost glycosylation in both A and C determinants **(Fig.4d-e)**. Unfavorable residues in determinant D are crucial in restricting human ACE2 from supporting NeoCoV binding and entry. However, hACE2 carrying the N338D mutation remains incapable of supporting MOW-15-22 or PnNL2018B entry **(Fig. S4)**. These results indicate that the ACE2 recognition mode utilized by these European ACE2-using merbecoviruses

differs considerably from NeoCoV and PDF-2180, which displayed a glycan-independent manner.

Discussion

Coronaviruses exhibit remarkable variations in RBD sequences, resulting in diverse receptor usage modes across different viruses[45]. Within the same genus or subgenus, coronaviruses often share very similar RBD core structures, but differences in receptor binding motifs (loops) can result in entirely different receptor usage[22,32,46]. Conversely, phylogenetically distant coronaviruses can convergently employ the same receptor during evolution. For example, receptor APN is shared by many alphacoronaviruses and deltacoronaviruses[46-49], while ACE2 serves as a common receptor for alphacoronaviruses and many sarbecoviruses[5,24,25,30]. Recently, we discovered ACE2 usage in merbecoviruses, NeoCoV and PDF-2180, expanded the ACE2 receptor usage to the third subgenus of coronaviruses[32].

The discovery of ACE2 usage in bat merbecoviruses closely related to MERS-CoV highlights the potential zoonotic risk associated with these viruses. Consequently, it becomes imperative to explore the global prevalence and distribution of ACE2-using merbecoviruses. Through scrutiny into RBM sequences and functional screening of receptor usage based on a mammalian ACE2 library, we identified two European bat coronaviruses, MOW-15-22 and PnNL2018B, as novel ACE2-utilizing merbecoviruses, despite prior studies proposing DPP4 usage based on molecular docking. Our findings strongly emphasize the need to verify *in silico* receptor usage predictions through functional binding and entry experiments, especially for coronaviruses with promiscuous receptor usage patterns.

In a previous report, we demonstrated that NeoCoV and PDF-2180 employ a glycan-assisted ACE2 interaction mode. However, glycan appears dispensable for ACE2 recognition by MOW-15-22 and PnNL2018B. Furthermore, it seems that the two other ACE2 determinants established by NeoCoV and PDF-2180 do not apply to the two European ACE2-using merbecoviruses. These discrepancies suggest a variation in ACE2 interaction mode. Revealing the cryo-EM structure of the viral MOW-15-22 RBD-Bat30 ACE2 complex in future studies could provide critical insights into the receptor recognition details of these viruses.

Compared to NeoCoV/PDF-2180, the two European ACE2-using merbecoviruses exhibit a narrow ACE2 recognition spectrum, with only a few bat ACE2 receptors facilitating pseudotyped

virus entry or RBD binding. It is likely that both viruses have a strict preference for their hosts' ACE2 receptors. Unfortunately, we were unable to test the ACE2 or DPP4 orthologues from this host species due to the unavailability of the complete genome sequence of *P. nathusii*. Neither of these viruses could use hACE2 based on their current sequences, and it remains unknown whether these viruses can acquire efficient recognition of hACE2 through point mutations in their RBM, akin to T510F in NeoCoV[32]. Overall, these two viruses exhibited lower spillover potential compared to NeoCoV and PDF-2180 at the receptor entry level.

The ACE2 usage was convergently established by different coronaviruses despite remarkable differences in their RBD structures. This ACE2 preference likely provides certain evolutionary advantages in transmission, as exemplified by the highly transmissible SARS-CoV-2 omicron strain [50,51]. However, a recent study reported that PnNL2180B (PN-βCoV) primarily exhibits intestinal tropism in its natural host, suggesting a potential fecal-oral route used by these viruses[36]. Given that airbrone transmission is the major route of all known ACE2-using human coronaviruses, it is important to investigate whether tissue tropism and transmission route changes when ACE2-using viruses jump from bats to humans.

Previous studies have revealed potential recombination events during the evolution of merbecoviruses, shedding light on the evolutionary history of MERS-CoV and related viruses[27,32]. Additionally, hypotheses have been proposed that ACE2-utilizing merbecoviruses might have arisen as a result of recombination between ancestral viruses of bats and hedgehogs. However, thus far, we have not detected any evidence of ACE2 usage by testing a hedgehog coronaviruses HKU31[29,32,52]. These observations raise interesting questions regarding the evolution trajectory of merbecoviruses and whether ACE2 or DPP4 receptor usage is the more ancestral trait for these viruses.

Our study significantly contributes to the understanding of ACE2-utilizing merbecoviruses by identifying and characterizing two novel ACE2-using merbecoviruses, expanding the known geographic distribution of these viruses to Europe in addition to Africa. The discovery of MOW-15-22 and PnNL2018B underscores the likelihood of many other yet-to-be-discovered ACE2-utilizing merbecoviruses, suggesting a potentially broader distribution than currently acknowledged Therefore, a comprehensive and expanded monitoring effort is essential to proactively detect and respond to potential outbreaks of ACE2-using merbecoviruses in humans. In-depth research on these viruses is warranted to provide valuable insights into their pathogenicity and

transmission abilities. Although we demonstrated that bat ACE2 recombinant proteins or broadly neutralizing antibodies can effectively block the entry of these viruses, future efforts of developing specific antibodies and vaccines are necessary to achieve better protection. Additionally, it is paramount to prepare effective antiviral drugs and vaccines to mitigate the risk of potential outbreaks caused by ACE2-using merbecoviruses.

Materials and methods

Cell lines

HEK293T (CRL-3216) and I1-Hybridoma (CRL-2700) cell line was acquired from the American Type Culture Collection (ATCC). These cells were maintained in Dulbecco's Modified Eagle Medium (DMEM, Monad, China) supplemented with 1% PS (Penicillin/Streptomycin) and 10% Fetal Bovine Serum. The I1-Hybridoma cell line, which produces a neutralizing antibody targeting the VSV glycoprotein (VSVG), was cultured in Minimum Essential Medium (MEM) with Earles's balances salts and 2.0 mM of L-glutamine (Gibico) and 10% FBS. All cell lines were cultured at 37°C with 5% CO_2 and underwent regular passage every 2-3 days.

Plasmids and vectors

Plasmids expressing wild-type (WT) or mutated bats ACE2 orthologues were constructed by inserting human codon-optimized sequences with/without specific mutations into a lentiviral transfer vector (pLVX-EF1a-Puro, Genewiz) with C-terminus 3×Flag tags (DYKDHD-G-DYKDHD-I-DYKDDDDK). For the expression of non-bat mammalian ACE2, human codon-optimized sequences of all ACE2 from non-bat mammals were cloned into a vector (pLVX-IRES-zsGreen) with a C-terminal Flag tag (DYKDDDDK). For pseudovirus production, human codon-optimized spike sequences of MOW-15-22 (USL83011.1), PnNL2018B (WDE20340.1), SARS-CoV-2 (YP_009724390.1) carrying D614G mutation, MERS-CoV (YP_009047204.1), HKU4 (AWH65899), NeoCoV (AGY29650.2) and HKU31 (QGA70692.1) were cloned into the pCAGGS vector with C-terminal deletions (13-15aa) for improving the pseudovirus assembly efficiency. For the expression of recombinant CoVs RBD-hFc fusion proteins, plasmids were constructed by inserting NeoCoV RBD (380-585aa), MOW-15-22 RBD (360-610aa),

PnNL2018B RBD (361-606aa) coding sequences into the pCAGGS vector containing an N-terminal CD5 secretion signal peptide (MPMGSLQPLATLYLLGMLVASVL) and a C-terminal hFc tag or hFc-twin-strep tandem tags for purification and detection. Plasmids expressing soluble bat ACE2 ectodomain proteins were generated by integrating *Pteronotus davyi* sequences (18-738 amino acids) into the pCAGGS vector, which included an N-terminal CD5 secretion signal peptide and a C-terminal twin-strep-3 × Flag tag (WSHPQFEKGGGSGGGSGGSAWSHPQFEKGGGRSDYKDHDGDYKDHDIDYKDDDDK).

Protein expression and purification

HEK293T cells were transfected with corresponding plasmids using GeneTwin reagent (Biomed, TG101-01). Subsequently, the culture medium of the transfected cells was replaced with the SMM 293-TII Expression Medium (Sino Biological, M293TII) 4-6 hours post-transfection, and the protein-containing supernatant was collected every three days for 2-3 batches. All recombinant RBD-hFc proteins were purified using Pierce Protein A/G Plus Agarose (Thermo Scientific, 20424). In general, hFc-fused proteins were captured by the Agarose, washed with wash buffer (100 mM Tris/HCl, pH 8.0, 150 mM NaCl, 1 mM EDTA), eluted using the Glycine buffer (100 mM in H_2O, pH 3.0), and immediately neutralized with 1/10 volume of 1M Tris-HCI, pH 8.0 (15568025, Thermo Scientific). Proteins with twin-strep tag were purified using Strep-Tactin XT 4Flow high-capacity resin (IBA, 2-5030-002), washed by wash buffer, and then eluted with buffer BXT (100 mM Tris/HCl, pH 8.0, 150 mM NaCl, 1 mM EDTA, 50 mM biotin). All eluted proteins were concentrated using Ultrafiltration tubes, buffer-changed to PBS, and stored at -80℃. Protein concentrations were determined by the Omni-Easy Instant BCA Protein Assay Kit (Epizyme, ZJ102).

RBD-hFc live-cell binding assays

The coronavirus RBD-hFc recombinant proteins were diluted in DMEM at indicated concentrations and incubated with HEK293T cells expressing different ACE2 for 30 mins at 37℃ at 36 hours post-transfection. Subsequently, cells were washed once with Hanks' Balanced Salt Solution (HBSS) and incubated with either 1 μg/mL of Alexa Fluor 488-conjugated goat anti-human IgG (Thermo Fisher Scientific; A11013) or DyLight 594-conjugated goat anti-human IgG (Thermo Fisher

Scientific; SA5-10136) diluted in HBSS/1% BSA for 1 hour at 37℃. After another round of washing with HBSS, the cell nuclei were stained with Hoechst 33342 (1:10,000 dilution in HBSS) for 30 mins at 37℃. The images were captured using a fluorescence microscope (MI52-N). The relative fluorescence intensities (RFU) of the stained cells were determined by a Varioskan LUX Multi-well Luminometer (Thermo Scientific). For flow cytometry analysis, HEK293T cells transiently expressing the indicated ACE2 orthologues were detached using 5 mM EDTA/PBS at 36 hours post-transfection. These cells were washed twice with cold PBS and incubated with MOW-15-22 or PnNL2018B RBD-hFc-twin-strep proteins at indicated concentrations at 4℃ for 30 minutes. Following this, cells were incubated with Alexa Fluor 488-conjugated goat anti-human IgG to stain the RBD (Thermo Fisher Scientific; A11013) at 4℃ for 1 hour. The cells were then fixed with 4% PFA, permeabilized with 0.25% Triton X-100, blocked with 1% BSA/PBS at 4℃, and then incubated with mouse antibody M2 (Sigma-Aldrich, F1804) diluted in PBS/1% BSA for 1 hour at 4℃, followed by incubation with Alexa Fluor 647-conjugated goat anti-mouse IgG (Thermo Fisher Scientific; A32728) diluted in 1% BSA/PBS for 1 hour at 4℃. For all samples, 10,000 ACE2-expressinglive cells (gated based on Flag-fluorescence intensity and SSC/FSC) were analyzed using a CytoFLEX Flow Cytometer (Beckman).

Biolayer interferometry (BLI) binding assay

Protein binding kinetics was analyzed using BLI assays with the Octet RED96 instrument (Molecular Devices) following the manufacturer's instructions. Generally, RBD-hFc recombinant proteins were diluted into the (20 μg/mL) and immobilized on the Protein A (ProA) biosensors (ForteBio, 18-5010), and then incubated with bat ACE2-ectodomain proteins, two-fold serial-diluted starting from 1000 nM, in a kinetic buffer (PBST). A control well containing only kinetic buffer (PBST) was used for background measurement. The kinetic parameters and binding affinities between the RBD-hFc and ACE2 were analyzed using Octet Data Analysis software 12.2.0.20 with curve-fitting kinetic analysis.

Pseudovirus production

VSV-dG-based pseudovirus carrying spike proteins from various coronaviruses were produced following a modified protocol as previously described[53]. Briefly, HEK293T cells were transfected

with plasmids expressing coronaviruses spike proteins. At 24 hours post-transfection, cells were transduced with 1.5×10^6 $TCID_{50}$ VSV-G glycoprotein-deficient VSV expressing GFP and firefly luciferase (VSV-dG-GFP-fLuc, constructed and produced in-house) diluted in DMEM with 8 μg/mL polybrene for 4-6 hours at 37 ℃. After three PBS washes, the culture medium was replenished with either DMEM+10% FBS or SMM 293-TII Expression Medium (Sino Biological, M293TII), along with an antibody (from I1-mouse hybridoma) targeting the VSV-glycoprotein to neutralize any remaining VSV-dG-GFP-fLuc. Twenty-four hours later, the pseudovirus containing supernatant was clarified through centrifugation at 12,000 rpm for 5 mins at 4℃, aliquoted, and stored at -80℃.

Pseudovirus entry assay

Pseudovirus entry assays were conducted using HEK293T cells transiently or stably expressing different ACE2 orthologues. Typically, $3x10^4$ trypsinized cells were incubated with pseudovirus (2×10^5 $TCID_{50}$/100 μL) in a 96-well plate to allow attachment and viral entry. Unless otherwise specified, pseudoviruses were treated with 10 μg/mL TPCK-trypsin (Sigma-Aldrich, T8802) before inoculation. Generally, pseudoviruses produced in serum-free SMM 293-TII Expression Medium were incubated with TPCK-treated trypsin for 10 mins at room temperature, and the proteolytic activity was neutralized by FBS in the culture medium for the cells. Intracellular luciferase activity was measured using the Bright-Glo Luciferase Assay Kit (Promega, E2620) and detected with a GloMax 20/20 Luminometer (Promega) at 18 hours post-infection.

Western blot

Cells expressing the indicated proteins were lysed in 1% TritonX/PBS+1 mM PMSF (Beyotime, ST506) for 10 mins at 4℃. The lysate was clarified after centrifugation of 12,000 rpm for 5 mins at 4℃, and then incubated at 98℃ for 10 mins after mixing with the 1/5 volume of 5×SDS loading buffer. Following gel electrophoresis and membrane transfer, the membranes were blocked with 5% skimmed milk in PBST for 2 hours at room temperature. Subsequently, the membrane was incubated with 1 μg/mL anti-Flag mAb (Sigma, F1804) or anti-β-tubulin (Immmuno Way, YM3030) mAb diluted in PBST containing 1% milk overnight at 4℃. After four washes with PBST, the blots were incubated with Horseradish peroxidase (HRP)-conjugated secondary antibody AffiniPure Goat

Anti-Mouse in 1% skim milk diluted in PBST and incubated for one hour at room temperature. Finally, the blots were washed four times again by PBST and visualized using an Omni-ECL Femto Light Chemiluminescence Kit (EpiZyme, SQ201) through a ChemiDoc MP Imaging System (Bio-Rad).

Immunofluorescence assay

Immunofluorescence assays were conducted to determine the expression levels of ACE2 orthologues with C-terminal fused 3×Flag tags. Generally, the transfected cells were fixed and permeabilized by incubation with 100% methanol for 10 mins at room temperature. Subsequently, the cells were incubated with a mouse antibody M2 (Sigma-Aldrich, F1804) diluted in PBS/1% BSA for one hour at 37℃. After a PBS wash, the cells were incubated with Alexa Fluor 594-conjugated goat anti-mouse IgG (Thermo Fisher Scientific, A32742) secondary antibody diluted in 1% BSA/PBS for one hour at 37℃. The images were captured and merged with a fluorescence microscope (Mshot, MI52-N) after the nucleus was stained blue with Hoechst 33342 reagent (1:5,000 dilution in PBS).

Bioinformatic and structural analysis

Sequence alignments of different bats ACE2 were performed using either the MUSCLE algorithm by MEGA-X (version 10.1.8) or ClustalW software (https://www.genome.jp/tools-bin/clustalw). Phylogenetic trees were generated using the maximal likelihood method in IQ-TREE (http://igtree.cibiv.univie.ac.at/) (1000 Bootstraps) and refined with iTOL (v6) (https://itol.embl.de/). The structures of MOW-15-22, PnNL2018B, and HKU31 RBD were predicted using alphaFold2.ipynb-Colaboratory. The structure of NeoCoV RBD & P.pip ACE2 complex (7WPO), MERS-CoV RBD (4KR0), HKU4 RBD (4QZV), MOW-15-22 RBD, HKU31 RBD, and PnNL2018B RBD were visualized and analyzed using the Chimera (V.1.14).

Statistical Analysis

Most experiments related to pseudovirus infection were conducted 2-3 times with 2-4 biological repeats. Representative results were shown. Data were presented by MEAN±SD, as indicated in the figure legends. Unpaired two-tailed t-tests were conducted for all statistical analyses using GraphPad Prism 8. $P<0.05$ was considered significant. * $p<0.05$, ** $p<0.01$, *** $p<0.005$, and **** $p<0.001$.

Acknowledgements

This study was supported by the National Natural Science Foundation (NSFC) of China projects (82322041, 32270164, 32070160), Fundamental Research Funds for the Central Universities (2042023kf0191, 2042022kf1188), Hubei Provincial Natural Science Foundation (2023AFA015).

Author contributions

H.Y. conceptualized the study design. L.C., and C.B.M. performed the experiments. C.B.M., C.L, H.Y., and Q.X. analyzed the data. C.B.M., C.L, H.Y., and Q.X. interpreted the results. H.Y. and C.B.M. wrote the initial drafts of the manuscript. H.Y., C.B.M., and C.L, revised the manuscript. C.B.M., C.L, H.Y., Q.X., X.Y.,Y.M.C.,J.Y.S.,P.L.,F.T., and M.L.H. commented on the manuscript. All authors read and approved the final manuscript.

Competing interests

The authors declare no competing interests.

Data availability

The authors declare that all data supporting the findings of this study are available with the paper and its supplementary information files.

Figure legend

Figure1

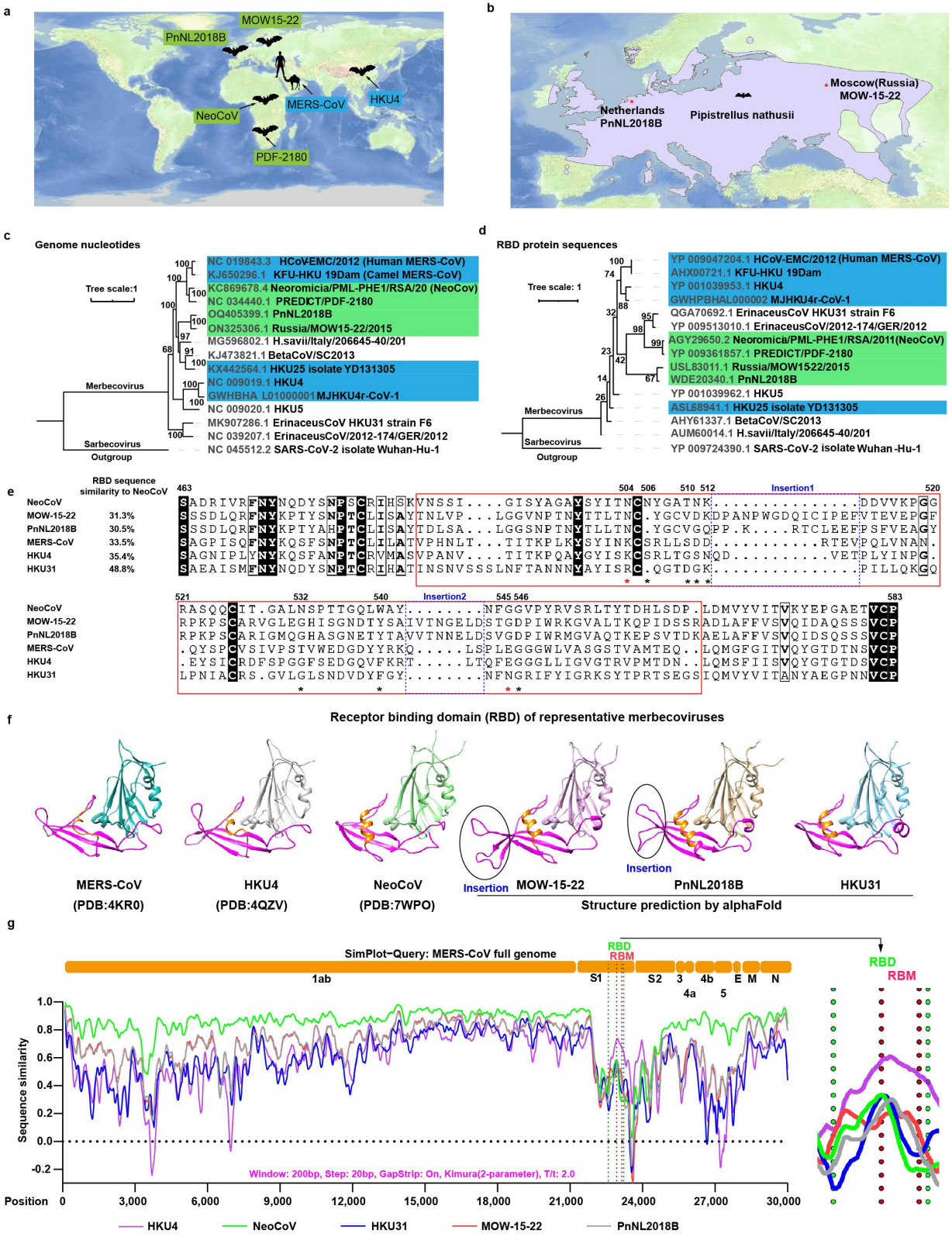

Fig.1 Analyses of MOW-15-22 and PnNL2018B RBD suggest potential ACE2 usage.

(a) Discovery locations and natural hosts of indicated merbecoviruses. Merbecoviruses that use DPP4 as their receptor are marked with a blue background, while those using ACE2 are highlighted

418 in green. **(b)** Geographical distribution of the *Pipistrelle nathusii* in Europe. The purple regions
419 represent its habitat, the data are retrived from the IUCN (International Union for Conservation of
420 Nature) Red List of Threatened Species, and the distribution chart is generated by Geoscene Pro. The
421 red arrows indicate the discovery location of MOW-15-22 and PnNL2018B.**(c-d)** Phylogenetic trees
422 of the representative merbecoviruses generated using complete genomes **(c)** or RBD protein
423 sequences **(d)** with the IQ-tree method. The background color distinguishes ACE2-using (green) and
424 DPP4-using (blue) merbecoviruses. The Sarbecovirus SARS-CoV-2 was set as the outgroup. **(e)** The
425 alignment of RBM sequences of indicated merbecoviruses generated using ClustalW and rendered
426 with ESPript. The putative receptor binding loops corresponding to NeoCoV RBM are highlighted in
427 a red dashed box, and two notable insertions in MOW-15-22 or PnNL2018B are indicated by the two
428 blue dashed boxes. Residues involved in crucial interactions between NeoCoV and P.pip ACE2 are
429 marked with asterisks, while conserved residues shared by NeoCoV, MOW-15-22, and PnNL2018B
430 are highlighted in red. **(f)** Cryo-EM Structures or AlphaFold-Predicted RBD structures of
431 representative merbecovirus. Pink indicates putative RBM, and orange represents the characterized
432 helix that may affect receptor usage. Two specific RBM insertions in MOW-15-22 and PnNL2018B
433 as mentioned in (e) are highlighted by blue circles. **(g)** Simplot analysis of the complete genome
434 nucleotide sequence similarity of five merbecoviruses analyzed based on the MERS-CoV genome.
435 Different ORF regions are indicated at the top. Green dashed lines mark RBD regions, and red
436 dashed lines mark RBM regions. The right panel represents the magnified charts of the RBD region.
437 T/t, transition/transversion ratio.
438
439

Figure2

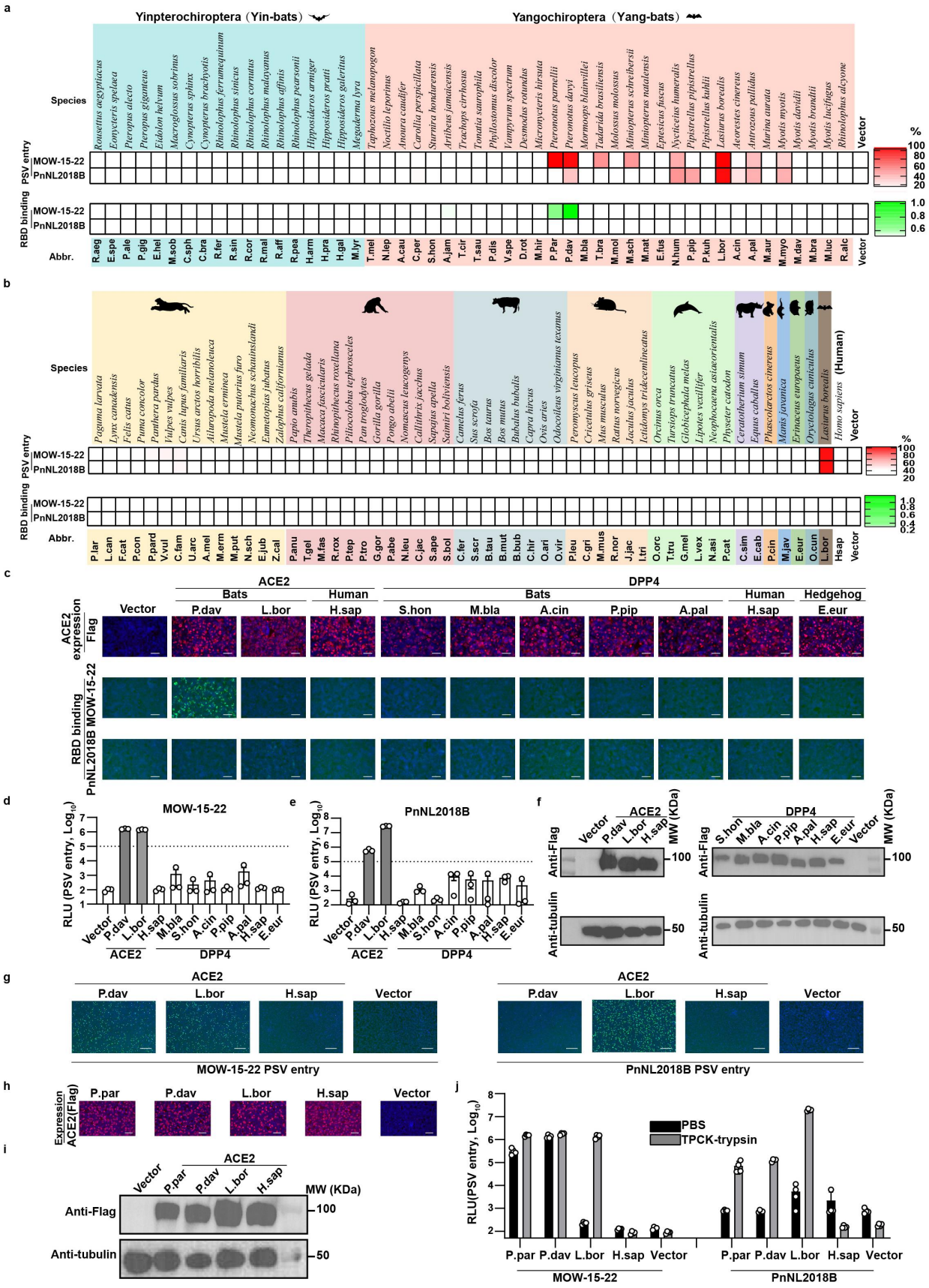

Fig.2 MOW-15-22 and PnNL2018B can use several bats ACE2 orthologues for efficient viral entry.

(a-b) Heat map representing MOW-15-22 and PnNL2018B RBD binding and PSV entry in HEK293T cells transiently expressing the various ACE2 orthologues from bats (**a**) or other mammals (**b**). Above: species names; Below: species abbreviations. Yinpterochiroptera (Yin-bats) and Yangchiroptera (Yang-bats) are indicated with cyan and pink backgrounds, respectively. Different mammal orders are marked with colored backgrounds, from left to right: Carnivora, Primates, Artiodactyla, Rodentia, Cetacea, Perissodactyla, Diprotodontia, Pholidota, Erinaceomorpha, and Lagomorpha. RBD binding efficiency is represented as mean fluorescence values in RBD binding assays, and the entry efficiency is normalized to the percentage of RLU values of the ACE2 orthologue with the highest RLU. (**c)** Expression levels of representative ACE2 and DPP4 receptors and the corresponding MOW-15-22 and PnNL2018B RBD binding intensity indicated by live-cell immunofluorescence. **(d-e)** PSV entry efficiency of MOW-15-22 **(d)** and PnNL2018B **(e)** in HEK293T expressing the indicated receptors. **(f)** Western blot analysis of receptor expression levels detecting C-terminal fused flag tags. **(g)** PSV entry efficiency of MOW-15-22 and PnNL2018B in HEK293T cells stably expressing P.dav, P.par, L.bor, and H.sap ACE2, as indicated by GFP intensity. **(h-i)** Immunofluorescence (**h**) and Western blot (**i**) detecting the ACE2 C-terminal flag tags of the diffenent ACE2 orthologues. **(j)** The PSV entry efficiency of MOW-15-22 and PnNL2018B with or without the presence of 10 μ g/mL TPCK-treated trypsin.

Data are presented as mean for n=4 biologically independent cells for **a** and **b.** Data are presented as mean ± SD for n=3 (**d, e**) or n=4 (**j**) biologically independent cells. Data representative of two independent experiments. The scale bars represent 100 μm for **c** and **g.** RLU: relative luciferase unit.

Figure3

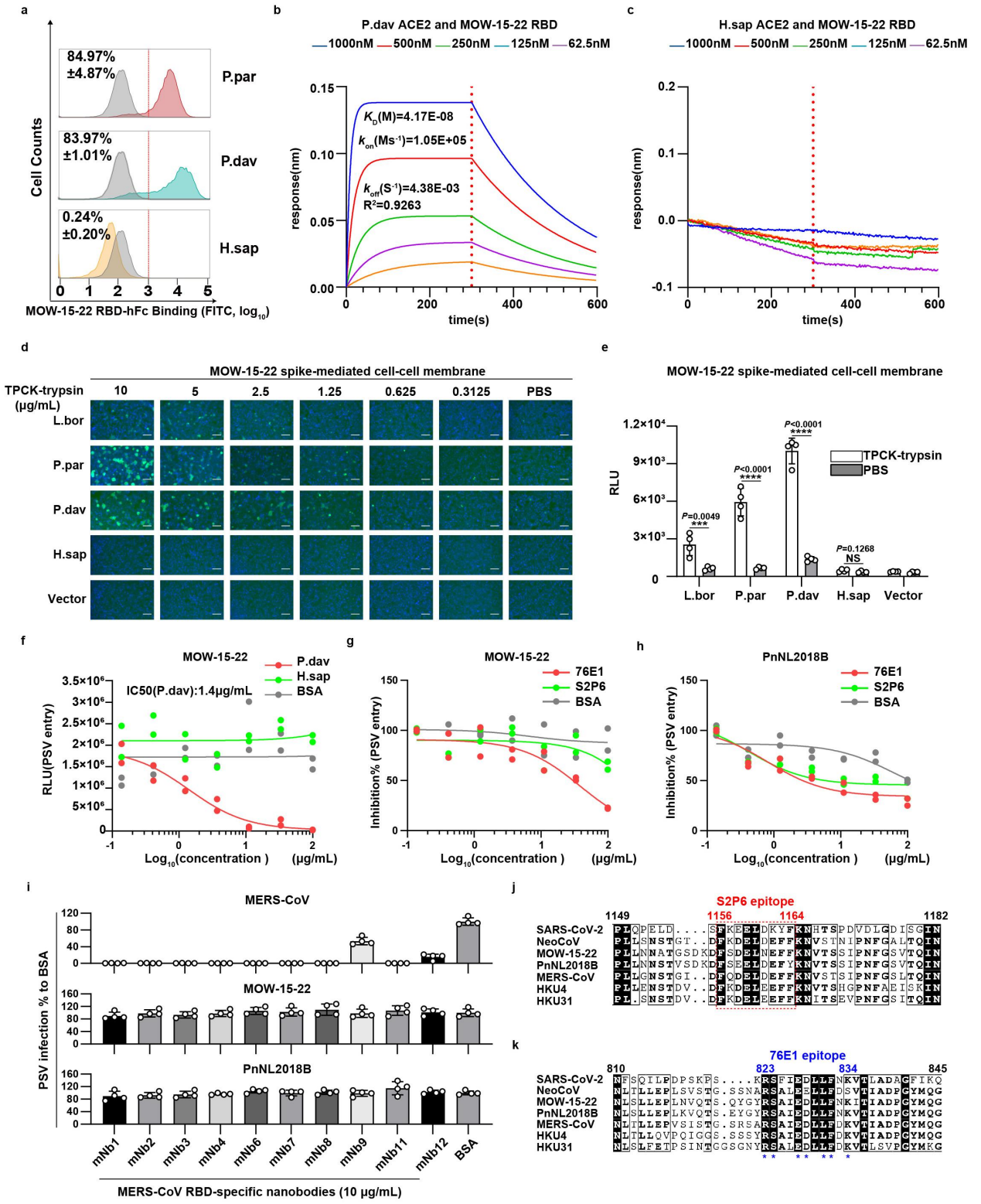

Fig. 3 Characterization of MOW-15-22 RBD binding, fusion, and viral entry mediated by bat ACE2.

（**a**）Flow cytometry analysis of MOW15-22 RBD-hFc binding with HEK293T cells transiently expressing the indicated ACE2 orthologues. The red dashed lines represent the threshold for positive

cells based on vector control. The positive ratio of the hFc staining signal is presented as Mean±SD. (**b-c**) Binding kinetics between MOW-15-22 RBD-hFc and the soluble recombinant P.dav **(b)** or H.sap **(c)** ACE2 ectodomain proteins analyzed by BLI assays. (**d-e**) MOW-15-22 spike mediated cell-cell membrane fusion in HEK293T stably expressing ACE2 orthologues in the presence of different concentration of TPCK-treated trypsin (two-fold serial-dilution from 10 μg/ml). Cell fusion efficiency is indicated by eGFP intensity (**d**) and live-cell Renilla luciferase activity (**e**) through the reconstitution of dual-split reporter proteins (DSP). (**f**) Dose-dependent inhibition of MOW-15-22 S-mediated entry by soluble ACE2 in HEK293T cells stably expressing P.dav ACE2. (**g-h**) Inhibitory activity of broadly neutralizing antibodies 76E1 and S2P6 against MOW-15-22 **(g)** and PnNL2018B **(h)** S pseudotyped viruses. **(i)** Inhibitory activity of MERS-CoV specific nanobodies (10 μ g/mL) against MERS-CoV, MOW-15-22 and PnNL2018B PSV entry. **(j-k)** Sequence alignment displaying the corresponding sequences of S2P6 **(j)** and 76E1 **(k)** epitopes in indicated coronavirus spikes. The red dashed box indicates the key epitope sequences of S2P6, and the blue asterisks indicate the key amino acid for 76E1 recognition. The numbering is based on SARS-CoV-2 spike sequences.

Data are presented as mean ± SD for n=3 biologically independent cells for **e** and n=4 **for i.** Data are shown as n=2 biologically independent cells for **f, g,** and **h.** Data representative of two independent experiments for **a-i.** RLU: relative light unit. The scale bars represent 100 μ m for **d**.

Figure4

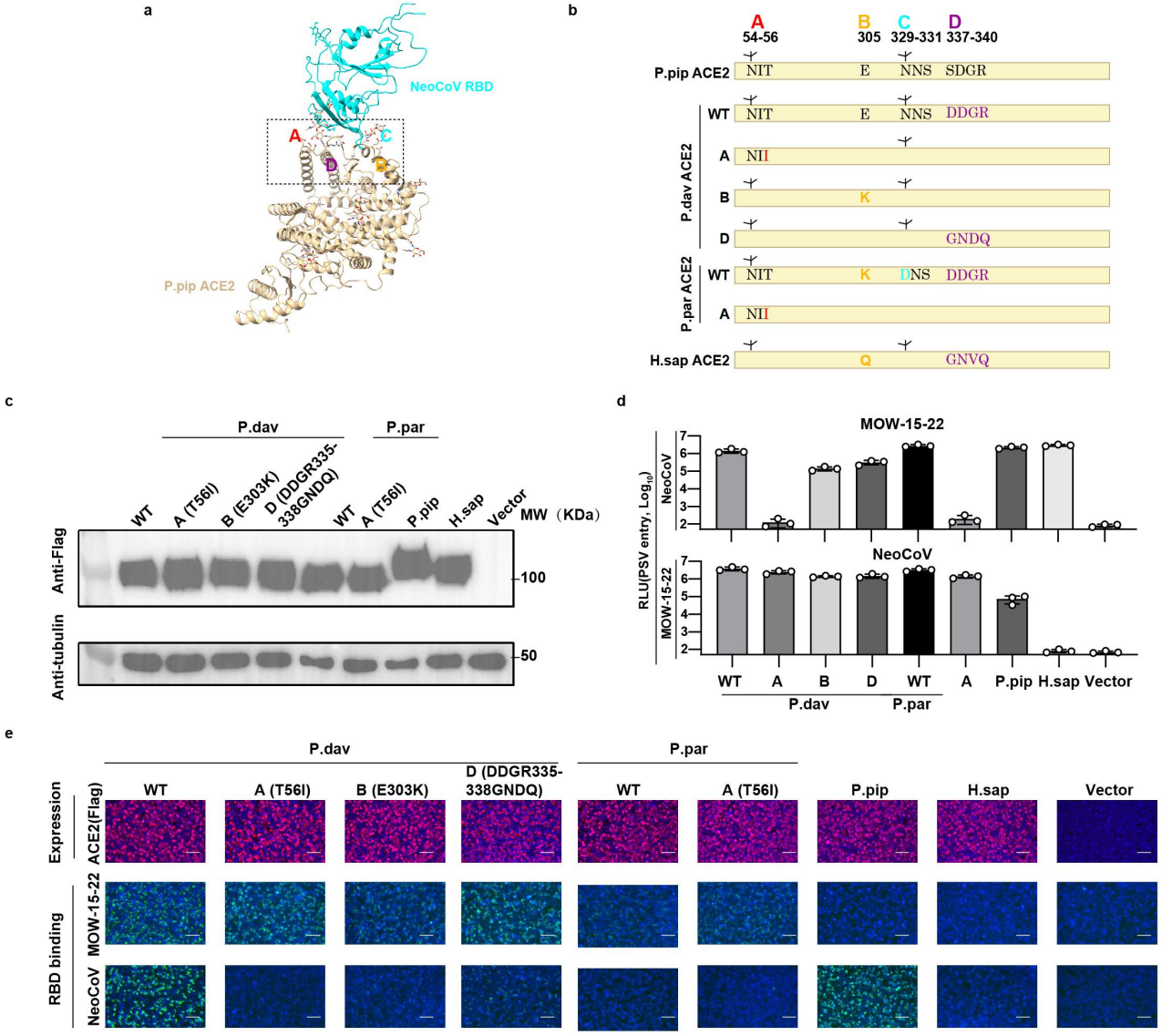

Fig. 4 MOW-15-22 utilizes a distinct glycan-independent binding mode to recognize ACE2 compared with NeoCoV.

(a) Structural view of four host range determinants (A-D) critical for species-specific ACE2 recognition by NeoCoV. **(b)** Schematic illustration of P.dav or P.par ACE2 mutants with indicated determinants replaced by Ppip ACE2 counterparts. The glycosylation sites in determinants A and C are demonstrated. **(c)** Western blot analyzing the expression of indicated WT and mutated ACE2 in HEK293T cells. **(d-e)** MOW-15-22 and NeoCoV PSV entry (d) and RBD binding efficiency(e) in HEK293T transiently expressing the indicated WT or mutants ACE2 orthologues. The expression level of the indicated ACE2 orthologues was verified by immunofluorescence (e, upper).

Data are presented as mean ± SD for n=3 biologically independent cells for **d.** Data representative of

two independent experiments for **c-e.** RLU: relative luciferase unit. Mw: molecular weight. The scale bars represent 100 μm for **e**.

1. Li, W. *et al.* Bats are natural reservoirs of SARS-like coronaviruses. *Science* **310**, 676-679 (2005).
2. Ge, X.Y. *et al.* Isolation and characterization of a bat SARS-like coronavirus that uses the ACE2 receptor. *Nature* **503**, 535-538 (2013).
3. Wang, Q. *et al.* Bat origins of MERS-CoV supported by bat coronavirus HKU4 usage of human receptor CD26. *Cell Host Microbe* **16**, 328-337 (2014).
4. Wong, A.C.P., Li, X., Lau, S.K.P. & Woo, P.C.Y. Global Epidemiology of Bat Coronaviruses. *Viruses* **11**, 174 (2019).
5. Zhou, P. *et al.* A pneumonia outbreak associated with a new coronavirus of probable bat origin. *Nature* **579**, 270-273 (2020).
6. Chen, L. *et al.* RNA based mNGS approach identifies a novel human coronavirus from two individual pneumonia cases in 2019 Wuhan outbreak. *Emerg Microbes Infect* **9**, 313-319 (2020).
7. Latinne, A. *et al.* Origin and cross-species transmission of bat coronaviruses in China. *Nat Commun* **11**, 4235 (2020).
8. Temmam, S. *et al.* Bat coronaviruses related to SARS-CoV-2 and infectious for human cells. *Nature* **604**, 330-336 (2022).
9. Ksiazek, T.G. *et al.* A novel coronavirus associated with severe acute respiratory syndrome. *N Engl J Med* **348**, 1953-1966 (2003).
10. Zaki, A.M., van Boheemen, S., Bestebroer, T.M., Osterhaus, A.D. & Fouchier, R.A. Isolation of a novel coronavirus from a man with pneumonia in Saudi Arabia. *N Engl J Med* **367**, 1814-1820 (2012).
11. WHO. MERS situation update; https://www.emro.who.int/health-topics/mers-cov/mers-outbreaks.html (2023).
12. Alagaili, A.N. *et al.* Middle East respiratory syndrome coronavirus infection in dromedary camels in Saudi Arabia. *mBio* **5**, e00884-14 (2014).
13. Meyer, B. *et al.* Antibodies against MERS coronavirus in dromedary camels, United Arab Emirates, 2003 and 2013. *Emerg Infect Dis* **20**, 552-9 (2014).
14. Memish, Z.A. *et al.* Human infection with MERS coronavirus after exposure to infected camels, Saudi Arabia, 2013. *Emerg Infect Dis* **20**, 1012-5 (2014).
15. Azhar, E.I. *et al.* Evidence for camel-to-human transmission of MERS coronavirus. *N Engl J Med* **370**, 2499-505 (2014).
16. Mohd, H.A., Al-Tawfiq, J.A. & Memish, Z.A. Middle East Respiratory Syndrome Coronavirus (MERS-CoV) origin and animal reservoir. *Virol J* **13**, 87 (2016).
17. Hassan, M.M. *et al.* NeoCoV Is Closer to MERS-CoV than SARS-CoV. *Infect Dis (Auckl)* **13**, 1178633720930711 (2020).
18. Lu, G., Wang, Q. & Gao, G.F. Bat-to-human: spike features determining 'host jump' of coronaviruses SARS-CoV, MERS-CoV, and beyond. *Trends Microbiol* **23**, 468-78 (2015).
19. Li, F. Structure, Function, and Evolution of Coronavirus Spike Proteins. *Annu Rev Virol* **3**, 237-261 (2016).
20. Maginnis, M.S. Virus-Receptor Interactions: The Key to Cellular Invasion. *J Mol Biol* **430**, 2590-2611 (2018).
21. Wan, Y., Shang, J., Graham, R., Baric, R.S. & Li, F. Receptor Recognition by the Novel Coronavirus from Wuhan: an Analysis Based on Decade-Long Structural Studies of SARS Coronavirus. *J Virol* **94**, e00127-20 (2020).

22. Li, F. Receptor recognition mechanisms of coronaviruses: a decade of structural studies. *J Virol* **89**, 1954-1964 (2015).
23. Tortorici, M.A. & Veesler, D. Structural insights into coronavirus entry. *Adv Virus Res* **105**, 93-116 (2019).
24. Li, W. *et al.* Angiotensin-converting enzyme 2 is a functional receptor for the SARS coronavirus. *Nature* **426**, 450-454 (2003).
25. Hofmann, H. *et al.* Human coronavirus NL63 employs the severe acute respiratory syndrome coronavirus receptor for cellular entry. *Proc Natl Acad Sci U S A* **102**, 7988-7993 (2005).
26. Ithete, N.L. *et al.* Close relative of human Middle East respiratory syndrome coronavirus in bat, South Africa. *Emerg Infect Dis* **19**, 1697-1699 (2013).
27. Corman, V.M. *et al.* Rooting the phylogenetic tree of middle East respiratory syndrome coronavirus by characterization of a conspecific virus from an African bat. *J Virol* **88**, 11297-11303 (2014).
28. Anthony, S.J. *et al.* Further Evidence for Bats as the Evolutionary Source of Middle East Respiratory Syndrome Coronavirus. *mBio* **8**, e00373-17 (2017).
29. Lau, S.K.P. *et al.* Identification of a Novel Betacoronavirus (Merbecovirus) in Amur Hedgehogs from China. *Viruses* **11**, 980 (2019).
30. Liu, K. *et al.* Binding and molecular basis of the bat coronavirus RaTG13 virus to ACE2 in humans and other species. *Cell* **184**, 3438-3451.e10 (2021).
31. (!!! INVALID CITATION !!!).
32. Xiong, Q. *et al.* Close relatives of MERS-CoV in bats use ACE2 as their functional receptors. *Nature* **612**, 748-757 (2022).
33. Ma, C. *et al.* Broad host tropism of ACE2-using MERS-related coronaviruses and determinants restricting viral recognition. *Cell Discov* **9**, 57 (2023).
34. Woo, P.C., Lau, S.K., Li, K.S., Tsang, A.K. & Yuen, K.Y. Genetic relatedness of the novel human group C betacoronavirus to Tylonycteris bat coronavirus HKU4 and Pipistrellus bat coronavirus HKU5. *Emerg Microbes Infect* **1**, e35 (2012).
35. Speranskaya, A.S. *et al.* Identification and Genetic Characterization of MERS-Related Coronavirus Isolated from Nathusius' Pipistrelle (Pipistrellus nathusii) near Zvenigorod (Moscow Region, Russia). *Int J Environ Res Public Health* **20**(2023).
36. Mols, V.C. *et al.* Intestinal Tropism of a Betacoronavirus (Merbecovirus) in Nathusius's Pipistrelle Bat (Pipistrellus nathusii), Its Natural Host. *J Virol* **97**, e0009923 (2023).
37. Reusken, C.B. *et al.* Circulation of group 2 coronaviruses in a bat species common to urban areas in Western Europe. *Vector Borne Zoonotic Dis* **10**, 785-91 (2010).
38. Iucnredlist.Org Available online: https://www.iucnredlist.org/species/17316/22132621.
39. Eurobats.Org Available online: https://www.eurobats.org/About_eurobats/Protected_bat_species/Pipistrellus_nathusii.
40. Moreno, A. *et al.* Detection and full genome characterization of two beta CoV viruses related to Middle East respiratory syndrome from bats in Italy. *Virol J* **14**, 239 (2017).
41. Yan, H. *et al.* ACE2 receptor usage reveals variation in susceptibility to SARS-CoV and SARS-CoV-2 infection among bat species. *Nat Ecol Evol* **5**, 600-608 (2021).
42. Menachery, V.D. *et al.* Trypsin Treatment Unlocks Barrier for Zoonotic Bat Coronavirus Infection. *J Virol* **94**(2020).
43. Pinto, D. *et al.* Broad betacoronavirus neutralization by a stem helix-specific human antibody. *Science* **373**, 1109-1116 (2021).
44. Sun, X. *et al.* Neutralization mechanism of a human antibody with pan-coronavirus reactivity including

584 SARS-CoV-2. *Nat Microbiol* **7**, 1063-1074 (2022).
585 45. Millet, J.K., Jaimes, J.A. & Whittaker, G.R. Molecular diversity of coronavirus host cell entry receptors. *FEMS*
586 *Microbiol Rev* **45**(2021).
587 46. Tortorici, M.A. *et al.* Structure, receptor recognition, and antigenicity of the human coronavirus
588 CCoV-HuPn-2018 spike glycoprotein. *Cell* **185**, 2279-2291.e17 (2022).
589 47. Yeager, C.L. *et al.* Human aminopeptidase N is a receptor for human coronavirus 229E. *Nature* **357**, 420-2
590 (1992).
591 48. Tresnan, D.B., Levis, R. & Holmes, K.V. Feline aminopeptidase N serves as a receptor for feline, canine, porcine,
592 and human coronaviruses in serogroup I. *J Virol* **70**, 8669-74 (1996).
593 49. Li, W. *et al.* Broad receptor engagement of an emerging global coronavirus may potentiate its diverse
594 cross-species transmissibility. *Proc Natl Acad Sci U S A* **115**, E5135-E5143 (2018).
595 50. Cameroni, E. *et al.* Broadly neutralizing antibodies overcome SARS-CoV-2 Omicron antigenic shift. *Nature* **602**,
596 664-670 (2022).
597 51. McCallum, M. *et al.* Structural basis of SARS-CoV-2 Omicron immune evasion and receptor engagement.
598 *Science* **375**, 864-868 (2022).
599 52. Corman, V.M. *et al.* Characterization of a novel betacoronavirus related to middle East respiratory syndrome
600 coronavirus in European hedgehogs. *J Virol* **88**, 717-724 (2014).
601 53. Whitt, M.A. Generation of VSV pseudotypes using recombinant DeltaG-VSV for studies on virus entry,
602 identification of entry inhibitors, and immune responses to vaccines. *J Virol Methods* **169**, 365-374 (2010).

603